

# Journal of Materials Chemistry B

Accepted Manuscript



This is an *Accepted Manuscript*, which has been through the Royal Society of Chemistry peer review process and has been accepted for publication.

*Accepted Manuscripts* are published online shortly after acceptance, before technical editing, formatting and proof reading. Using this free service, authors can make their results available to the community, in citable form, before we publish the edited article. We will replace this *Accepted Manuscript* with the edited and formatted *Advance Article* as soon as it is available.

You can find more information about *Accepted Manuscripts* in the [Information for Authors](#).

Please note that technical editing may introduce minor changes to the text and/or graphics, which may alter content. The journal's standard [Terms & Conditions](#) and the [Ethical guidelines](#) still apply. In no event shall the Royal Society of Chemistry be held responsible for any errors or omissions in this *Accepted Manuscript* or any consequences arising from the use of any information it contains.

## ARTICLE

## A Novel Zwitterionic Bioceramic with Dual Antibacterial Capability

Cite this: DOI: 10.1039/x0xx00000x

Montserrat Colilla,<sup>a,b,c,\*</sup> Marina Martínez-Carmona,<sup>a,b,c</sup> Sandra Sánchez-Salcedo,<sup>a,b,c</sup> M. Luisa Ruiz-González,<sup>c,d</sup> José M. González-Calbet<sup>c,d</sup> and María Vallet-Regí<sup>a,b,c,\*</sup>

Received 00th January 2012,  
Accepted 00th January 2012

DOI: 10.1039/x0xx00000x

[www.rsc.org/](http://www.rsc.org/)

A novel *zwitterionic* SBA-15 type bioceramic with dual antibacterial capability has been synthesized. The co-condensation route has been employed to functionalize SBA-15 with primary and secondary amine groups. The resulting material exhibits textural and nanostructural properties comparable to that of pure silica SBA-15, as confirmed by XRD and HR-TEM and N<sub>2</sub> adsorption porosimetry. The presence of  $-\text{NH}_3^{\oplus}/-\text{SiO}^{\ominus}$  and  $>\text{NH}_2^{\oplus}/-\text{SiO}^{\ominus}$  *zwitterionic* pairs onto the material surface is evidenced by FTIR and <sup>1</sup>H→<sup>13</sup>C CP/MAS solid state NMR. The homogeneous distribution of this *zwitterionic* pairs agrees with the results derived from STEM-EDS studies. ζ-potential measurements indicate that the *zwitterionic* nature of this material is preserved at the physiological pH of 7.4. *In vitro* bacterial assays using *S. aureus* demonstrates that *zwitterionic* material is capable of inhibiting in a 99.9% the bacterial adhesion compared to pure silica SBA-15. Moreover, cephalexin loading and delivery assays indicate that *zwitterionic* sample is capable of releasing antibiotic molecules over long time periods. This dual antibacterial capability, *i.e.* antibiofouling and bactericidal, opens up promising expectations for the treatment of bone implant infections.

### Introduction

Despite considerable recent biomedical and engineering progresses, infection remains one of the most severe and devastating complications associated to the use of implants for the treatment of bone diseases and fractures.<sup>1-4</sup> In fact, bone implants are ideal substrates for bacteria colonization, since it is well-known that microorganisms prefer to colonize a solid substrate than dwell in a planktonic state.<sup>5</sup> Following an initial colonization bacteria grow and form communities called biofilms, which critically compromise the functionality and performance of the implant itself. Once mature bacterial biofilm has established, conventional medical therapies based on systemic administration of antibiotics are not efficient and implant removal often constitutes the only possibility to eradicate the infection. This causes high morbidity and patient

suffering and also constitutes an enormous cost for the national health systems.<sup>2,3</sup>

Currently, much research effort is being dedicated to design advanced bioceramics that exhibit antibacterial surfaces, *i.e.* surfaces capable of reducing the extent of attachment and proliferation of bacteria.<sup>6</sup> Antibacterial surfaces may repel or resist the initial attachment of bacteria by either exhibiting an antibiofouling effect or by inactivating any cells coming into contact with the surface, therefore exhibiting a bactericidal effect.<sup>6</sup> Among the chemical strategies to design antibiofouling or bacterial antiadhesive surfaces, functionalization with hydrophilic,<sup>7</sup> antimicrobial<sup>8</sup> and *zwitterionic* polymers and their derivatives<sup>9,10</sup> have been reported. Recently, *zwitterionization* of bioceramics has been reported as a promising strategy to develop antibiofouling surfaces.<sup>11-13</sup> In addition, bactericidal surfaces have been prepared by using diverse approaches such using coatings containing silver and silver nanoparticles,<sup>14</sup>

grafting of antimicrobial peptides<sup>15,16</sup> and quaternary ammonium compounds<sup>17</sup> or loading bioceramic matrices with antibiotics.<sup>18-24</sup> An innovative strategy to provide bioceramics of bactericidal capability consisted in grafting aminosilane derivatives to the surface of mesoporous silica materials, which were subsequently reacted or “charged” with NO. The NO release from the resulting materials led to biofilm eradication meanwhile exhibiting low *in vitro* cytotoxicity.<sup>25,26</sup>

The current challenge is to design antibacterial surfaces capable of combining antibiofouling and bactericidal capabilities for the dual treatment of implant infections. However, only a few strategies have been reported to attain this goal, which are based in the combination of polymeric surfaces capable of switching between attacking (e.g. cationic) and defending (e.g. *zwitterionic*) forms.<sup>27,28</sup>

Herein, we report the design and synthesis of a new nanostructured *zwitterionic* SBA-15 type bioceramic with dual antibacterial capability for the treatment of bone implant infections. The antibiofouling capability comes from the intrinsic *zwitterionic* nature of the surface, whereas the bactericidal potential results from its capability to host antibiotic drugs into the mesopores. *Zwitterionic* SBA-15 has been prepared by using an alkoxy silane bearing primary and secondary amine groups and following the co-condensation route. Co-condensation offers several advantages compared to post-grafting functionalization.<sup>29</sup> Since DAMO is a direct component of the silica matrix, pore blocking is not a problem using co-condensation method. Besides, co-condensation usually lead to functionalized matrices where the organic units are generally more homogeneously distributed than in materials synthesized by the post-grafting process. Finally, the number of SiOH groups available to form *zwitterionic* species with amino groups from DAMO is higher when using the co-condensation route. Post-grafting functionalization would involve spending a great amount of surface SiOH groups of SBA-15 in forming covalent linkages (Si-O-Si) with DAMO. This would originate positively charged surfaces at the physiological pH of 7.4, as it has been reported elsewhere.<sup>30</sup> Co-condensation route permitted incorporating  $-\text{NH}_3^+/\text{-SiO}^-$  and  $>\text{NH}_2^+/\text{-SiO}^-$  *zwitterionic* pairs onto the material surface, as evidenced by Fourier transform infrared spectroscopy (FTIR) and <sup>13</sup>C solid state nuclear magnetic resonance (NMR). A deep study by high resolution transmission electron microscopy (HR-TEM) and energy dispersive scanning and transmission electron spectroscopy (STEM) coupled to energy dispersive X-ray spectroscopy (EDS) allowed investigating the nanostructure of the resulting materials and the distribution of functional groups in mesoporous crystals.  $\zeta$ -potential measurements were performed to determine the surface charge properties of this material vs. pH and to study if its *zwitterionic* nature was preserved under physiological conditions (pH~7.4). The antibacterial adhesion capability of *zwitterionic* SBA-15 compared to pure silica SBA-15 was *in vitro* tested using *S. aureus*, a microorganism usually involved in bone implant infections. Moreover, *in vitro* loading and release assays using

cephalexin, a broad spectrum antibiotic used to treat common infections, were carried out.

## Materials and Methods

### Synthesis of SBA-15 type mesoporous materials

Functionalized SBA-15 type silica mesoporous material exhibiting both primary and secondary amine groups, denoted as SBA-Zwitter, was synthesized by co-condensation route using N-(2-aminoethyl)-3-aminopropyl-trimethoxysilane (DAMO, 97% wt., ABCR). Briefly, 8.0 g of Pluronic® P123 block copolymer (PEO<sub>20</sub>PPO<sub>70</sub>PEO<sub>20</sub>) kindly provided by BASF Co.) was added to a mixture of 276 ml of H<sub>2</sub>O and 20.6 mL of concentrated HCl (37% wt., Aldrich).<sup>31</sup> The solution was moderately stirred for 24 h at 35 °C until total surfactant dissolution. Then, 15 mL of tetraethyl orthosilicate (TEOS, 98% wt., Aldrich) was added. After *ca.* 20 min a white powder appeared. Then, 1.64 mL of DAMO previously solved in 8.2 mL of isopropanol was dropwise added to the suspension. Mixtures were kept under magnetic stirring at 35 °C during 24 h and then sealed in glass beakers and heated at 100 °C for further 24 h. Finally, the obtained products were filtered, washed with deionized water, and then dried at 60 °C for 24 h. Then, the surfactant was removed by extraction.<sup>32</sup> For this purpose, 1 g of mesoporous material was soaked into 100 mL of an isoctane/ethanol (3:2) mixture (isoctane, ≥99.5% wt., Aldrich; ethanol, 95%, Panreac) and kept under magnetic stirring at room temperature for 48 h. Afterward, sample was filtered and then submitted to a second extraction process by soaking powder into 120 mL of an acetone/water (1:1) mixture (acetone, QP, Panreac) during 24 h at room temperature under magnetic stirring. After the extraction processes samples were left to dry into vacuum oven during 24 h to ensure total solvent removal. For comparison, pure silica SBA-15 was also synthesized. Table 1 displays the molar compositions of the precursor sols used for the synthesis of the different mesoporous materials.

**Table 1.** Different molar compositions of the precursors used during the synthesis of the different mesoporous materials.

Sample	TEOS	DAMO	P123	HCl	H <sub>2</sub> O
SBA-15	1	0	0.017	3.4	208
SBA-Zwitter	0.90	0.10	0.017	3.4	208

### Characterization of materials

The structural characteristics of the resulting materials were determined by powdered X-ray diffraction (XRD) in a Philips X'Pert diffractometer (Eindhoven, The Netherlands) equipped with CuK $\alpha$  (40 kV, 20 mA) over the range from 0.6 to 8.0° with a step of 0.02° and a contact time of 5 s. Electron microscopy was carried out in a JEOL 3000FEG transmission electron microscope operating at 300 kV and fitted with a X-ray energy dispersive spectrometer (EDS) (Oxford Instruments) and a Scanning Transmission Electron Microscopy (STEM) system.

The textural properties of samples were determined by N<sub>2</sub> adsorption porosimetry. The N<sub>2</sub> adsorption/desorption analyses were carried out at -196 °C on a Micromeritics ASAP2020 analyzer (Micromeritics Co., Norcross, USA). In all cases, 50-70 mg of material was degassed at 90 °C for 24 h under a vacuum lower than 0.3 kPa before the analysis. The surface area was determined using the Brunauer-Emmett-Teller (BET) method.<sup>33</sup> The total pore volume was estimated from the amount adsorbed at a relative pressure of 0.97. The estimation of microporous and mesoporous fractions to the total pore volume was performed by the t-plot method.<sup>34</sup> The average mesopore size (D<sub>p</sub>) was obtained from the maximum of the pore size distribution calculated from the adsorption branch of the isotherm using the BJH method.<sup>35</sup> The wall thickness (t<sub>wall</sub>) was calculated by means of the expression t<sub>wall</sub> = a<sub>0</sub> - D<sub>p</sub>, where a<sub>0</sub> is the unit cell parameter calculated from the d<sub>10</sub> value of XRD using the expression a<sub>0</sub> = d<sub>10</sub> · 2/√3.<sup>36</sup> To assess the possible existence of micropores (pore diameter <2 nm) in samples, the t-plot method was employed, which allowed the estimation of the microporous fraction contribution (V<sub>μP</sub>) to the total pore volume.

The existence of functional groups and their chemical nature were investigated by FTIR in a Thermo Nicolet Nexus spectrometer equipped with a Goldengate attenuated total reflectance (ATR) device (Thermo scientific, USA). Quantitative determination of amino groups in SBA-Zwitter sample sourced from DAMO was carried out by CHNS elemental chemical analysis in a Perkin-Elmer 2400CHNS thermo analyzer. The amount of residual surfactant amount in samples was calculated from CHNS analytic results and thermal analyses (TG and DTA). Thermal analyses were carried out under a dynamic air atmosphere between 30 and 950 °C (flow rate of 50 mL/min with a heating rate of 10 °C/min) using a Perkin-Elmer Diamond analyzer (Perkin-Elmer, USA).

To investigate the cross-linking degree and the amount of silanol groups present in the synthesized materials <sup>29</sup>Si magic angle spinning (MAS) solid-state nuclear magnetic resonance (NMR) measurements were performed in a Bruker AV-400-WB spectrometer (Karlsruhe, Germany) operating at 79.49 MHz. Solid samples were placed in a 4-mm zirconia rotor and spun at 10 kHz. Chemical shifts (δ) of <sup>29</sup>Si were externally referred to 3-trimethylsilyl-1-propanesulfonic acid sodium salt (DDS) at δ=0.0 ppm. Time periods between successive accumulations were 5 ms and ca. 15000 scans were collected. The population of silanol groups per mol of silica was calculated from the relative population of silanol and geminal species, and divided by the weight per mol of silica materials (eq 1).<sup>37</sup> The weight is derived from the relative populations and effective molecular weights (EMW) of the silanol, geminal, and siloxane species. The effective molecular weight of each species (EMWQ) is defined as the sum of the molecular weight of the atoms contributing to each species, with the oxygen atoms in the siloxane bridges (Si-O-Si) that connect the species counted by half. The equation is:

$$[\text{SiOH}] = \frac{(2 \times \%Q^2) + \%Q^3}{(\%Q^1 \times \text{EMW}_Q)} \quad (\text{Eq. 1})$$

where [SiOH] is the silanol group concentration in mol/g and %Q<sup>i</sup> is the relative population of species Q<sup>i</sup> (Q<sup>2</sup>, Q<sup>3</sup>, and Q<sup>4</sup>).

<sup>1</sup>H→<sup>13</sup>C CP (cross-polarization)/MAS solid-state NMR measurements were performed to evaluate the different carbon environments in the synthesized samples. Spectrometer frequency was set to 75.45 MHz and samples were spun at 12 kHz. Chemical shift values were referenced to glycine. Time period between successive accumulations was 3 ms and the number of scans was ca. 15000.

To evaluate the behavior of materials, regarding their surface charge properties in aqueous media, zeta-potential (ζ) measurements at different pH values were performed on a Malvern Zetasizer Nano Series instrument coupled to a MPT-2 multipurpose titrator from Malvern Instruments Ltd (UK). For this purpose, 5 mg of each powdered sample mesoporous was added to 5 mL of KCl 10 mM (used as the supporting electrolyte) and the pH was adjusted by adding appropriate volumes of 0.10 M HCl or 0.10 M KOH solutions.

#### *In vitro* bacterial adhesion assays

Bacterial adhesion assays on SBA-Zwitter and SBA-15 using Gram positive *Staphylococcus aureus* (American Type Culture Collection, ATCC 28213) were performed under static conditions, as commonly reported in the literature.<sup>12,38-41</sup>

To perform the bacterial adhesion experiments on the different powdered materials, disk-shaped pieces of 6 mm diameter and 1 mm height were prepared by compacting fractions of 20 mg of dried powders using 2.75 MPa uniaxial pressure. Prior to adhesion assay, samples were sterilized by UV irradiation for 7 min on each side of the piece.

*S. aureus* were grown to a mid-logarithmic phase in Todd Hewitt broth (THB) medium (Sigma-Aldrich, USA) at 37 °C under orbital stirring at 100 rpm until the optical density as measured at 600 nm reached 1 in a UV-VIS spectrometer (UV-530, Bonsai technologies, Spain). At this point, the bacteria from culture were collected by centrifugation (Labofuge 400 centrifuge, Thermo Scientific, USA) at 1500 rpm for 10 min at room temperature, washed three times with sterile phosphate buffer saline (PBS, Sigma-Aldrich, pH 7.4) and resuspended in 10 mL of PBS. The number of bacteria were retrospectively confirmed by plating serial dilutions of the starting inocula in agar Petri dishes (Tryptic Soy Agar, TSA 90MM plate agar, BD Difco, USA). The chosen dilution was that allowing the direct counting of colony-forming units (CFUs). The chosen dilution was that of concentration 1.5 × 10<sup>6</sup> cells per mL. The different disk-shaped samples were soaked in 1 mL of bacterial suspension of 1.5 × 10<sup>6</sup> cells per mL and incubated at 37 °C under orbital stirring at 100 rpm for 90 min. Then, the samples were aseptically removed and rinsed three times with PBS to eliminate any free bacteria. Afterwards, two different

experiments were carried out, which are described in the next sub-sections.

**QUANTIFICATION OF ADHERED BACTERIA.** With the aim of quantifying the adhered bacteria, each disk was placed in a 1 mL of PBS in Eppendorf vial (Nirco, Spain) followed by 30 s sonication in a low power bath sonicator (Selecta, Spain). This sonication process was carried out three times, assuming that 99.9% of adhered bacteria were removed.<sup>42</sup> Then, 100  $\mu$ l of each sonication product was cultivated on TSA plates, followed by incubation at 37 °C overnight. Determination of the number of CFUs resulting from the overall sum of the three sonication processes allowed the determination of the number of bacteria initially adhered onto the disks. Experiments were performed by triplicate. To be able to express bacteria adhesion as CFUs per unit surface, it is necessary to know the porosity accessible to bacteria. For this purpose, the microstructure of disk-shaped pieces was investigated by scanning electron microscopy (SEM) using a field emission JEOL JSM-6335F microscope (Tokyo, Japan) at an acceleration voltage of 10 kV. Moreover, the porosity of disks was measured by mercury intrusion porosimetry in a Micromeritics Autopore IV 3500 device (Micromeritics Instrument Corporation, Norcross, GA, USA). The pore size distributions were obtained after applying the Washburn equation to the values of the filling pressure to obtain the equivalent pore sizes, which were plotted versus the cumulative volumes of Hg intruded into the pores at each pressure point.<sup>43</sup> The different size ranges were then defined and the surface area for each one was reported by AutoPore IV software. The number of CFUs per  $\text{cm}^2$  was calculated by normalization of the counted CFUs as a function of the surface area of the disk-shaped pieces in the 1–600  $\mu$ m range.

Data obtained from bacterial adhesion assays were expressed as means  $\pm$  standard deviations of the independent experiments indicated in each case. Statistical analysis was performed using the Statistical Package for the Social Sciences (SPSS) version 19 software. Statistical comparisons were made by analysis of variance (ANOVA). Scheffé test was used for post hoc evaluation of difference among groups. In all statistical evaluations,  $p < 0.05$  was considered as statistically significant.

**VISUALIZATION OF ADHERED BACTERIA BY CONFOCAL MICROSCOPY.** To visualize the bacteria adhered to the different surfaces, samples were stained with Live/Dead® BacLight™ bacterial viability and counting kit.<sup>44</sup> This kit utilizes a mixture of two nucleic acid stains, green fluorescent SYTO 9 dye and red-fluorescent propidium iodide (PI). Following the protocol provided in the kit, a mixture of SYTO 9 (live bacteria/green) and PI (dead bacteria/red) dyes were added to the disk-shaped samples soaked in fresh PBS and kept in contact during 15 min in the darkness. After that time, samples were washed with PBS and immediately observed in a Biorad MC1025 confocal laser scanning microscope (Bio-Rad Laboratories, CA, USA). SYTO 9 was excited at 480/500 nm and the emitted fluorescence was measured at 500 nm. On the other hand, PI was excited at 490/635 nm and the emitted fluorescence was measured at 618

nm. Each experiment was carried out in three specimens. Three zones of each specimen of a surface of 95.4  $\mu$ m  $\times$  95.4  $\mu$ m were captured in each image. Images showing surface areas covered with dead (red) and live (green) bacteria were optimized using ImageJ software (National Institute of Health Bethesda, MD, USA).

#### **In vitro cephalixin loading and release assays**

Cephalixin (CPX) loading assays were performed by soaking 250 mg of powder samples in 10 mL of a 20 mM CPX solution in water (pH = 6) during 40 hours under magnetic stirring. Then, samples were filtered, gently washed with water and dried at room temperature under vacuum for further 24 hours. The presence of CPX in powdered samples was assessed by FTIR spectroscopy and the amount of drug loaded was determined by CHNS elemental chemical analysis.

To carry out in vitro CPX release assays, 35 mg of each drug-loaded powder sample was compacted into disks of 6 mm in diameter and 2 mm in height by using uniaxial pressure at 2.75 MPa. Then, disks were hung in screw caps using platinum wires and soaked into tubes containing 2 mL of PBS. The solution was kept at 37 °C, and to avoid limitations of the delivery rate by external diffusion constraints, continuous orbital stirring at 150 rpm was maintained during the assays. After determined periods of time, samples were removed from PBS and placed in tubes containing 2 mL of fresh PBS. The cumulative CPX released was determined by UV-Vis in a Unicam UV500 spectrometer (Gemini BV, Germany). For this purpose, absorbance was measured at 251 nm. CPX solutions in PBS with concentrations in the 0.01–0.2 mg/mL were used for calibration. The curve was linear with a relationship of Absorbance = 13.95  $\times$  [CPX] (correlation coefficient = 0.998). The apparent drug release was normalized to the amount of drug loaded within the samples to observe the relative amount of drug release. CPX concentration was determined from the average of the readings from three different samples (N = 3), and data were presented as mean  $\pm$  standard deviation.

#### **Agar disk-diffusion tests of cephalixin-loaded materials**

Agar disk diffusion tests (ADT) were used to examine the antibacterial effect of CPX-loaded materials. To carry out ADT, 20 mg of each CPX-loaded powder sample was compacted into disks of 6 mm in diameter and 2 mm in height by using uniaxial pressure at 2.75 MPa. For comparison, ADT were also performed using CPX-free disk-shaped samples. Prior to adhesion assay, samples were sterilized by UV irradiation for 7 min on each side of the piece. The surface of solid agar in Petri dishes was inoculated with a suspension of *S. aureus* bacterial culture with a cell concentration of  $1.3 \times 10^{10}$  bacteria/mL. After that, disks were placed on the bacteria inoculated agar plates followed by incubation at 37°C for 24 hours. After that, bacterial inhibition zone size was measured as (outer diameter of inhibition zone – disk diameter)/2.<sup>45</sup> Each study was performed by triplicate.

**Table 2.** Characteristics of the materials synthesized in this work obtained by N<sub>2</sub> adsorption, XRD, CHN elemental analysis, <sup>29</sup>Si MAS solid state NMR and ζ-Potential measurements.

Sample	S <sub>BET</sub> (m <sup>2</sup> /g)	V <sub>T</sub> (cm <sup>3</sup> /g)	V <sub>μP</sub> (cm <sup>3</sup> /g)	D <sub>P</sub> (nm)	a <sub>0</sub> (nm)	t <sub>wall</sub> (nm)	-(CH <sub>2</sub> ) <sub>3</sub> NH(CH <sub>2</sub> ) <sub>2</sub> NH <sub>2</sub> /nm <sup>2</sup>	SiOH /nm <sup>2</sup>	IEP
SBA-15	553	0.80	0.0021	9.8	11.9	2.1	-	10.9	4.2 ± 0.1
SBA-Zwitter	490	0.77	~ 0	9.2	12.4	3.2	0.61	13.8	7.4 ± 0.1

S<sub>BET</sub> is the surface area determined by using the BET method between the relative pressures (P/P<sub>0</sub>) 0.05-0.25. V<sub>P</sub> and V<sub>μP</sub> are respectively, the total pore volume and micropore volume obtained using the *t*-plot method. The total pore volume was estimated from the amount of N<sub>2</sub> adsorbed at a relative pressure of 0.97. D<sub>P</sub> is the pore diameter calculated by means of the BJH method from the adsorption branch of the isotherm. a<sub>0</sub> is the unit cell parameter calculated by XRD, being a<sub>0</sub>=2/√3·d<sub>10</sub>. t<sub>wall</sub> is the wall thickness calculated using the equation t<sub>wall</sub> = a<sub>0</sub> - D<sub>P</sub>. The number of -NH(CH<sub>2</sub>)<sub>2</sub>NH<sub>2</sub> groups was calculated on the basis of elemental chemical analysis. The number of silanol groups (SiOH) was determined by single pulse <sup>29</sup>Si solid state NMR spectroscopy, as described in the experimental section. IEP point is the isoelectric point of samples determined by ζ-potential measurements.

## Results and Discussion

### Characterization of mesoporous materials

Structural characterization by XRD and TEM indicates that all samples exhibit ordered mesoporous arrangements typical of SBA-15 structure (Fig. 1.A and Fig. 2).<sup>31</sup> XRD patterns at small angles exhibit well resolved peaks at 1:3<sup>1/2</sup>:2 d-spacing ratios, which can be indexed as 10, 11, and 20 reflections, respectively, of a 2D-hexagonal structure with *p6mm* plain group similar to that of SBA-15 (Fig. 1.A). TEM images and their corresponding FT (Fast Fourier Transforms) for synthesized samples, acquired with the electron beam perpendicular and parallel to the cylindrical channels, confirm a honeycomb mesoporous arrangement typical of SBA-15 (Fig. 2). EDS analysis was performed during the TEM observation. Si and O peaks clearly appear for both samples (Fig. 2e and 2g) while the asymmetry on the O peak for SBA-Zwitter indicates the presence of nitrogen (Fig. 2 g).

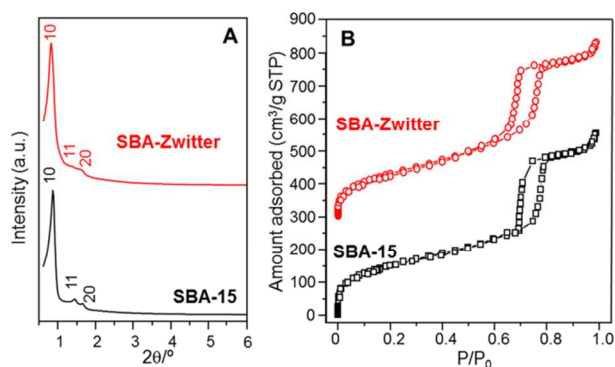


**Fig. 1.** Characteristics of SBA-15 and SBA-Zwitter samples obtained by A) XRD and B) N<sub>2</sub> adsorption measurements; the isotherm for sample SBA-Zwitter was vertically offset by 300 cm<sup>3</sup>/g STP.

N<sub>2</sub> adsorption isotherms (Fig. 1.B) can be identified as type IV isotherms according to the IUPAC classification, which are typical of mesoporous solids.<sup>34</sup> The presence of H1 type hysteresis loops in the mesopore range indicates the existence

of open-ended cylindrical mesopores with narrow pore size distributions, which are characteristic of SBA-15.<sup>34,36</sup> The main textural features derived from the appropriate treatment of N<sub>2</sub> adsorption data are summarized in Table 2. Both SBA-15 and SBA-Zwitter samples exhibit good textural properties, with high surface areas (S<sub>BET</sub> ~ 500 m<sup>2</sup>/g), great pore volumes (V<sub>P</sub> ~ 0.8 cm<sup>3</sup>/g) and large pore diameters (D<sub>P</sub> ~ 9 nm). The slight decrease in the S<sub>BET</sub>, V<sub>P</sub> and D<sub>P</sub> values and the increase in the wall thickness (t<sub>wall</sub>) of SBA-Zwitter compared to those of pure silica SBA-15 can be ascribed to the incorporation of organic functions into the mesoporous silica framework.

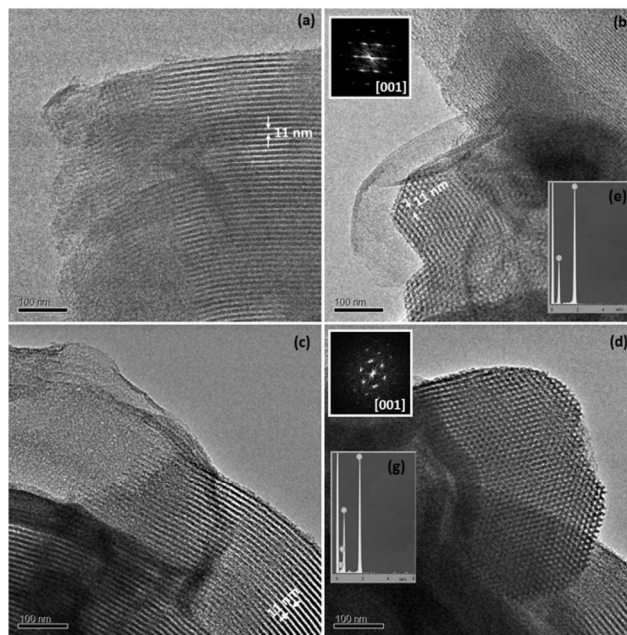


**Fig. 2.** (a) and (c) TEM images acquired with the electron beam perpendicular to the mesoporous channels for SBA-15 and SBA-Zwitter samples, respectively; (b) and (d) TEM images acquired with the electron beam parallel to the mesoporous channels for SBA-15 and SBA-Zwitter samples, respectively. The corresponding FT's are included as insets; (e) EDS spectrum characteristic of SBA-15 sample; EDS spectrum characteristic of SBA-Zwitter sample.

Besides, SBA-Zwitter shows negligible micropore volume, which suggests that the grafted groups block such a contribution upon functionalization by lining the mesopore

surface. The noticeable free mesopore area and pore volume indicate that these materials can be used as host matrices to load large amounts of biologically active molecules, such as drugs, peptides and relatively small proteins, for subsequent controlled release.<sup>23,46</sup>

Once confirmed the ordered mesoporous structure of these materials, the chemical nature of samples was investigated by using FTIR, CHNS elemental chemical analysis and STEM-EDX. Fig. 3 displays FTIR spectra of samples. As it can be observed, all spectra show a broad band around 3400  $\text{cm}^{-1}$  corresponding to the overlapping of the O–H stretching bands of hydrogen-bonded water molecules (H–O–H) and SiO–H stretching of surface silanols hydrogen bonded to molecular water (SiO–H...OH<sub>2</sub>).

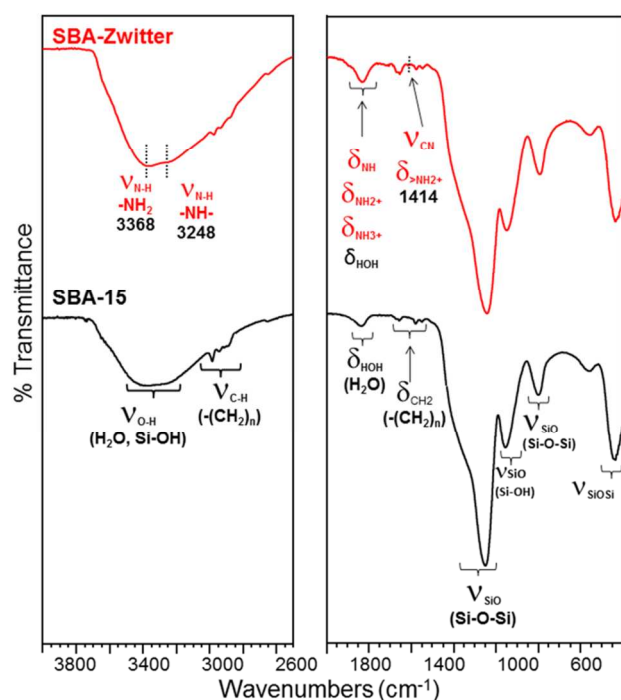


Fig. 3. FTIR spectra (4000–2500  $\text{cm}^{-1}$  and 1800–400  $\text{cm}^{-1}$  regions) of SBA-15 and SBA-Zwitter samples.

The O–H bending vibration mode of this adsorbed water is responsible for the band centered at 1630  $\text{cm}^{-1}$ . In addition, the Si–O in-plane stretching vibrations of the silanol Si–OH groups appear at 960  $\text{cm}^{-1}$ , whose reasonably high intensity accounts for the relatively low polymerization degree of the silica matrices, as it is demonstrated by <sup>29</sup>Si MAS solid state NMR study (*vide infra*). The intense silicon-oxygen covalent bond vibrations appearing in the 1100–1000  $\text{cm}^{-1}$  range indicate the existence of a silica network, where oxygen atoms play the role of bridges between two silicon atoms. In addition, the symmetric stretching vibration of Si–O–Si and its bending mode appear at *ca.* 800 and 440  $\text{cm}^{-1}$ , respectively.<sup>47</sup> The low energy band at 560  $\text{cm}^{-1}$  is assigned to Si–O stretching of the silica network defects. In addition, several bands in the 2980–2850  $\text{cm}^{-1}$  range, assigned to the C–H symmetric and

antisymmetric stretching vibrations of –CH<sub>2</sub>– groups of the residual surfactant, are also distinguished. There are several vibration bands ascribed to bending vibrations of –CH<sub>2</sub> groups of the template in the 1500–1330  $\text{cm}^{-1}$  range. The relative intensity of such bands is higher in the spectrum of SBA-Zwitter than that of SBA-15 due to the presence of alkyl groups of DAMO. FTIR spectrum of SBA-Zwitter displays additional bands at 3368 and 3248  $\text{cm}^{-1}$  that are assigned to stretching vibrations of primary (NH<sub>2</sub>) and secondary (NH) amino groups, respectively. The strong absorption in the 3600–3400  $\text{cm}^{-1}$  range appearing in the spectrum is attributable to the presence of water in the solid. The increase in the intensity and broadening of the band centered at 1630  $\text{cm}^{-1}$  from 1680–1600  $\text{cm}^{-1}$  for SBA-15 to 1680–1560  $\text{cm}^{-1}$  for SBA-Zwitter points to the presence of a new band overlapping  $\delta_{\text{HOH}}$  vibration of adsorbed water molecules. This band, centered at *ca.* 1580  $\text{cm}^{-1}$  can be assigned to  $\delta_{\text{NH}}$ ,  $\delta_{\text{NH}_2^+}$ , and  $\delta_{\text{NH}_3^+}$ , although  $\delta_{\text{CH}_2}$  bands of Si–CH<sub>2</sub> groups of DAMO could be also present in the same interval.<sup>48</sup> Moreover, at 1414  $\text{cm}^{-1}$  there is a characteristic band of  $\delta_{\text{NH}_2^+}$  within the  $\nu_{\text{CN}}$  band of DAMO. These two bands suggest that SBA-Zwitter sample contain protonated amino groups, forming *zwitterionic* species via deprotonation of adjacent silanol groups (–SiO<sup>–</sup>).

TG-DTA and CHNS elemental analyses allowed determining the amount of residual surfactant, being less than 5% wt. in both samples. This small amount of residual surfactant did not have any bactericidal effect, as derived from *in vitro* assays with *S. aureus* (*vide infra*). Elemental chemical analysis revealed that the number of functional groups present in SBA-Zwitter sample was 0.61 [–(CH<sub>2</sub>)<sub>3</sub>NH(CH<sub>2</sub>)<sub>2</sub>NH<sub>2</sub>]/nm<sup>2</sup>, which is almost a half of the nominal value of 1.2 groups/nm<sup>2</sup> that corresponds to the 0.90/0.10 TEOS/DAMO molar ratio used during the synthesis. Such finding points to an upper limit of functional groups from DAMO per square nanometer capable of being incorporated into the silica framework without provoking the loss of the mesostructural order. This is a well-known characteristic of mesoporous samples functionalized using the one-pot or co-condensation method.<sup>29</sup> This fact was demonstrated by carrying out the functionalization of SBA-15 with DAMO via co-condensation route and employing different TEOS/DAMO molar ratios than that used to synthesize SBA-Zwitter (results not shown). Thus, when using a 0.95/0.05 TEOS/DAMO molar ratio, 0.65 [–(CH<sub>2</sub>)<sub>3</sub>NH(CH<sub>2</sub>)<sub>2</sub>NH<sub>2</sub>]/nm<sup>2</sup> were determined in the resulting SBA-15 type ordered mesoporous material. On the contrary, when using a higher nominal functionalization degree (0.85/0.15 TEOS/DAMO molar ratio) the resulting sample lacked of structural order. In this case the organic functions from DAMO would be somehow disrupting the silica framework and hindering the formation of ordered mesostructures.

To further investigate if there is a homogeneous distribution of N within mesoporous crystals, chemical mapping by means of EDS spectroscopy under STEM configuration of samples were carried out. EDS spectrum of pure silica SBA-15 displays typical signals of Si and O. Fig. 4a shows STEM image of SBA-Zwitter taken with the electron beam perpendicular to the

mesochannels. The corresponding EDS spectrum displays two additional maxima that can be attributed to C and N from DAMO (Fig. 4b). An EDS study was carried out by selecting different mesoporous crystals and recording N, O and Si maps from appropriate  $K\alpha$  signals (Fig. 4c-e). Mapping of the square region highlighted in STEM image, shows a very weak N signal (previously observed in the punctual EDS analysis in Fig. 2), suggesting that N of  $[-(\text{CH}_2)_3\text{NH}(\text{CH}_2)_2\text{NH}_2]$  groups from DAMO is randomly and homogeneously distributed within the mesoporous silica framework. This fact can be ascribed to the synthetic approach followed to functionalize SBA-15, *i.e.* co-condensation, as it has been widely reported.<sup>29</sup> These findings together with the results derived from FTIR and  $^{13}\text{C}$  NMR spectroscopies (*vide infra*) accounts for the homogeneous distribution of  $>\text{NH}_2^{\oplus}\cdots^{\ominus}\text{OSi-}$  and  $-\text{NH}_3^{\oplus}\cdots^{\ominus}\text{OSi-}$  zwitterionic species in the surface of SBA-Zwitter sample.

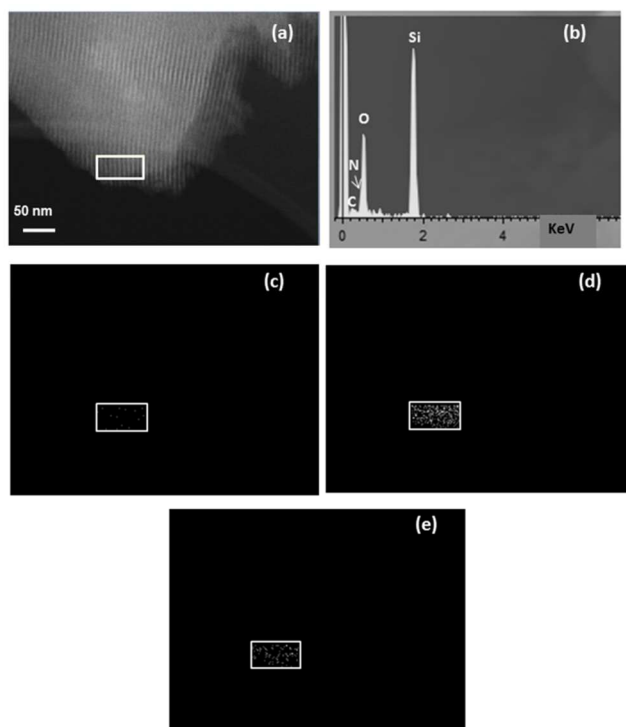


**Fig. 4.** (a) STEM image of SBA-Zwitter taken with the electron beam perpendicular to the mesochannels. (b) Corresponding EDS spectrum. (c-e) N, O and Si maps from appropriate  $K\alpha$  signals of the square region highlighted in (a).

$^{29}\text{Si}$  MAS-NMR measurements were performed to assess the chemical grafting of organosiloxane to the silica networks. Tetra-functional silicon centers were named with the conventional  $Q^n$  notation where Q refers to  $[(\text{SiO})_n\text{Si}(\text{OX})_{4-n}]$  units, being  $n$  the number of bridging oxygen atoms surrounding the central silicon atom and  $X = \text{H}$  or  $\text{CH}_2\text{CH}_3$ . Similarly, tri-functional silicon centers were named with the conventional  $T^m$  notation where T refers to  $[(\text{SiO})_m\text{RSi}(\text{OX})_{3-m}]$  units, being  $m$  the number of bridging oxygen atoms surrounding the central silicon atom,  $X = \text{H}$  or  $\text{CH}_3$  and  $R =$

$(\text{CH}_2)_3\text{NH}(\text{CH}_2)_2\text{NH}_2$  of DAMO. The relative populations of silicon environments were calculated by deconvolution of the  $^{29}\text{Si}$  NMR spectra into individual Gaussian peaks. All the resonance signals from the spectra and the corresponding relative peak areas are displayed in Table 3. Spectra of both samples display resonances at *ca.* -84, -93, -103 and -112 ppm assigned to silicon atoms in  $Q^1$ ,  $Q^2$ ,  $Q^3$  and  $Q^4$  environments (Fig. 5). The spectral analysis suggests that the surface Si-OH groups are associated as  $Q^1$ ,  $Q^2$  and  $Q^3$  structural units in pure-silica SBA-15. The relative high amount of silanol groups can be explained by the method used for the surfactant removal, *i.e.* solvent extraction, which leads to matrices with a lower condensation degree than those resulting from surfactant calcination.<sup>29</sup> These finding agrees with the results derived from FTIR, where vibration bands of relatively high intensity due to silanol groups were observed in the spectra.

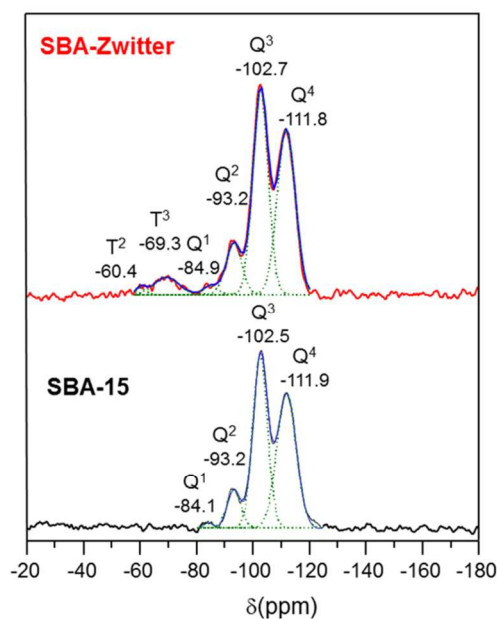


**Fig. 5.**  $^{29}\text{Si}$  MAS NMR spectra of SBA-15 and SBA-Zwitter samples. The component peaks obtained from spectral deconvolutions are displayed by green dotted lines.

$^{29}\text{Si}$  MAS solid state NMR spectrum of SBA-Zwitter sample shows two additional down-field peaks assigned to organosiloxane species  $T^2$  at *ca.* -60 and  $T^3$  at *ca.* -69 ppm. This confirms the existence of covalent bonds between the silica surface and the organic groups, even if some degree of self-condensation cannot be overruled. The relative abundance of  $T^n$  species allowed to calculate a molar functionalization degree (%F) of 6%, which is almost a half of the nominal one (10%). This result is in good agreement with the results derived from elemental chemical analysis above discussed, where the number of  $-(\text{CH}_2)_3\text{NH}(\text{CH}_2)_2\text{NH}_2$  groups per square nanometer in samples (0.61) were almost a half of the nominal value (1.2).

**Table 3.** Peak area (%) of T<sup>m</sup> and Q<sup>n</sup> units from deconvoluting the <sup>29</sup>Si MAS NMR spectra SBA-15 and SBA-Zwitter samples. Molar functionalization degree (%F) of SBA-Zwitter sample is also displayed.

Sample	Peak area (%) of Q <sup>n</sup> and T <sup>m</sup> signals						%F*
	T <sup>2</sup>	T <sup>3</sup>	Q <sup>1</sup>	Q <sup>2</sup>	Q <sup>3</sup>	Q <sup>4</sup>	
SBA-15	-	-	1	9	45	45	-
SBA-Zwitter	1	5	2	11	42	39	6

\*The molar functionalization degree of samples (%F) was calculated according to the formula %F = T<sup>m</sup>/(Q<sup>n</sup>+T<sup>m</sup>).

<sup>1</sup>H-<sup>13</sup>C CP/MAS solid state NMR spectra were collected to confirm the functionalization of mesoporous materials and to get information about the ionization state and hydrogen bonding environment of amine groups from DAMO.

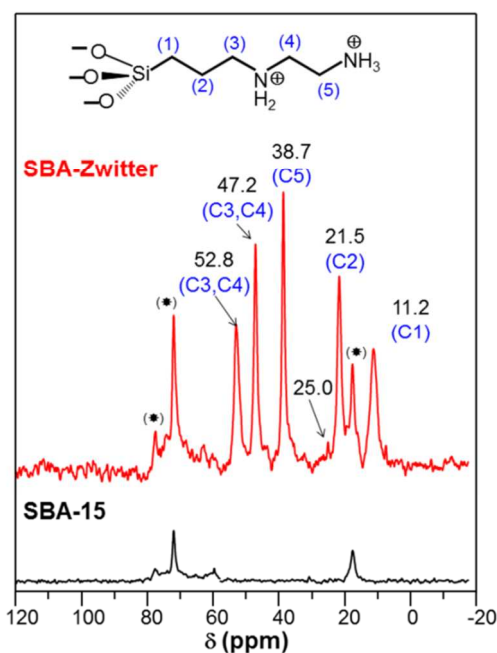


**Fig. 6.** <sup>1</sup>H-<sup>13</sup>C CP/MAS solid state NMR spectra of SBA-15 and SBA-Zwitter samples.

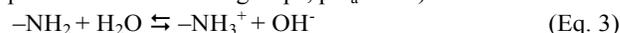
As expected, signals attributed to residual surfactant are found in <sup>13</sup>C NMR spectrum of both, pure silica SBA-15 and SBA-Zwitter materials (Fig. 6), in agreement with results derived from elemental chemical analyses and TG-DTA measurements. SBA-Zwitter spectrum exhibits several signals that can be assigned to the different carbon atoms from DAMO. Signals at 47.2 and 52.8 are indistinctly attributed to carbons C3 and C4 of DAMO that, being close to protonation centers (-NH<sub>2</sub><sup>+</sup> and -NH<sub>3</sub><sup>+</sup>), may be present in different chemical environments originating multiple signals.<sup>49</sup> The well-defined signals at 38.7, 21.5 and 11.2 ppm are respectively ascribed to C5, C2 and C1 carbons of DAMO. The resonance at 21.5 ppm, representing C2 exhibits a larger shift change toward upper field relative to pure DAMO (ca. 26 ppm) due to the protonation of amine groups in SBA-Zwitter.<sup>50</sup> Nonetheless, a weak resonance at 25 ppm can be distinguish, which would correspond to the C2 carbon of non-protonated DAMO. These findings support the presence of

>NH<sub>2</sub><sup>+</sup>...<sup>-</sup>OSi- and -NH<sub>3</sub><sup>+</sup>...<sup>-</sup>OSi- *zwitterionic* species in SBA-Zwitter sample, although a very small population of amine groups could remain non-protonated.

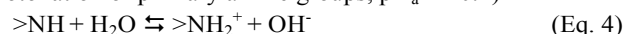
Once the chemical nature of SBA-Zwitter was investigated, their surface charge as a function of pH was evaluated by recording ζ-potential measurements at different pH values. The resulting ζ-potential vs. pH plots are displayed in Fig. 7. The different equilibria accounting for the surface charges experimentally observed are displayed below:<sup>30</sup>



(deprotonation of silanol groups, pK<sub>a</sub> = 4.8)



(protonation of primary amine groups, pK<sub>a</sub> = 10.4)



(protonation of secondary amine groups, pK<sub>a</sub> = 9.2)

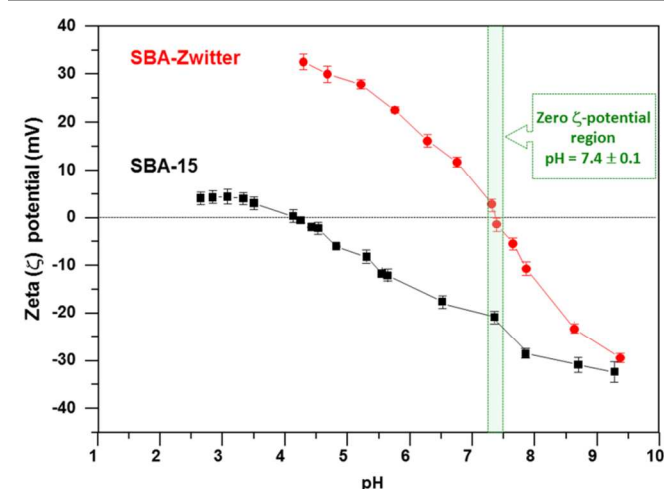


**Fig. 7.** ζ-potential vs pH plots of SBA-15 and SBA-Zwitter samples. The shaded area indicates the zero ζ-potential region for sample SBA-Zwitter.

The isoelectric point (IEP) of SBA-15, which is tightly related to the zero surface charge point, is ca. 4.2, in agreement with the results reported elsewhere.<sup>11,30</sup> The high number of silanol groups on the surface of SBA-15, 10.9 SiOH per square nanometer (Table 2) would be the responsible of this behavior. Silanol groups, which exhibit weak acidic Brønsted character, would be deprotonated as -Si-O<sup>-</sup> groups at pH values above 4.2, (Eq. 2) providing a negative surface charge in the pH range of biological interest. On the other hand, SBA-Zwitter exhibits an IEP of ca. 7.4, which match to the physiological pH. Below such pH, the presence of protonated amino groups from DAMO (Eqs. 3 and 4) provides mesoporous material of a positive surface charge. At pH 7.4 the concomitant presence of -Si-O<sup>-</sup> and protonated amino groups (>NH<sub>2</sub><sup>+</sup> and -NH<sub>3</sub><sup>+</sup>) forming *zwitterionic* pairs results in a zero surface charge. Finally, at pH higher than 7.4 the greater number of silanol groups (13.8 SiOH/nm<sup>2</sup>) compared to that of diamine moieties (0.61 - (CH<sub>2</sub>)<sub>3</sub>NH(CH<sub>2</sub>)<sub>2</sub>NH<sub>2</sub>- groups per nm<sup>2</sup>) (Table 2), creates a net negative surface charge.

It has been demonstrated that SBA-Zwitter exhibits >NH<sub>2</sub><sup>+</sup>/-SiO<sup>-</sup> and -NH<sub>3</sub><sup>+</sup>/-SiO<sup>-</sup> *zwitterionic* pairs onto its surface.

Moreover,  $\zeta$ -potential measurements in aqueous media point to the preservation of the *zwitterionic* nature at the physiological pH of 7.4. The next step would be to evaluate the capability of SBA-Zwitter to inhibit bacterial adhesion compared to pure silica SBA-15. For this purpose, *in vitro* bacterial adhesion assays at pH 7.4 using *S. aureus* were carried out, at it is discussed in the next section. Moreover, the good textural and distinctive chemical characteristics of SBA-Zwitter make this material excellent candidate to host therapeutic molecules and release them in a sustained fashion. Therefore, the *in vitro* drug loading and release capabilities of SBA-Zwitter compared to SBA-15 were also evaluated, as it is described below.

### In vitro bacterial adhesion assays

To further evaluate the behavior of SBA-Zwitter material towards bacterial adhesion, *in vitro* assays were carried out by soaking disk-shaped materials during 90 min at 37 °C in a suspension of *S. aureus* in PBS at pH of 7.4, as described in the experimental section. For comparison, *in vitro* bacterial adhesion assays using SBA-15 were also performed. With the aim of normalizing the number of CFUs per surface unit, the microstructure of disk-shaped samples was investigated. SEM micrographs of disk-shaped SBA-15 and SBA-Zwitter show the characteristic microstructure for SBA-15 type mesoporous materials, *i.e.* a material consisting of many rope-like domains with relatively uniform sizes of around 1  $\mu\text{m}$ , which are aggregated into wheat-like macrostructures (Fig. S1, see supporting information).<sup>31</sup> Hg intrusion porosimetry measurements reveal the presence of intergranular pores with sizes in the 100–600  $\mu\text{m}$  and 5–600  $\mu\text{m}$  ranges for SBA-15 and SBA-Zwitter, respectively. The total surface area within such ranges of macroporosity was 20  $\text{cm}^2/\text{g}$  for SBA-15 and 160  $\text{cm}^2/\text{g}$  for SBA-Zwitter, being the higher porosity of the latter attributable to the presence of organic moieties during the synthetic procedure. Therefore, the degrees of *S. aureus* adhesion for the different material surfaces, expressed as CFUs per square centimetre, are displayed as histograms in Fig. 8. The adhered bacteria was *ca.*  $2.88 \pm 0.53$  and  $(2.16 \pm 0.66) \times 10^3$  CFUs/ $\text{cm}^2$  onto SBA-Zwitter and SBA-15 sample, respectively. The statistic one-way ANOVA tests show that the bacterial adhesion values for the different surfaces were significantly different ( $p < 0.01$ ). *S. aureus* adhesion on SBA-Zwitter samples significantly decreased *ca.* 99.9% compared to SBA-15 samples. This effect can be attributed to the presence of  $>\text{NH}_2^{\oplus}/-\text{SiO}^{\ominus}$  and  $-\text{NH}_3^{\oplus}/-\text{SiO}^{\ominus}$  *zwitterionic* pairs into the material surface of SBA-Zwitter, which would provide its surface of ultralow-fouling capability towards *S. aureus* bacteria adhesion. The mechanism of inhibition of bacterial adhesion on *zwitterionic* surfaces is not fully understood. However, it can be explained as an increase of surface hydration via electrostatic interactions in addition to hydrogen bonding due to of a great polarity of the charged functional groups.<sup>51</sup> Thus, water molecules on the *zwitterionic* surface

would create a strong repulsive force on the bacteria as they approach the surface.

The visualization of adhered bacteria into the different surfaces was performed by confocal microscopy using fluorescence based Live/Dead® BacLight™ bacterial viability test. This assay provides useful information about the membrane integrity of *S. aureus*. Fig. 8 shows images collected by confocal fluorescence microscopy after 90 minutes of bacterial adhesion assay onto disk-shaped SBA-15 and SBA-Zwitter surfaces. The surface of pure silica SBA-15, used as reference, is colonized by *S. aureus* bacteria with intact cell membranes, as derived from bright green fluorescent signals.

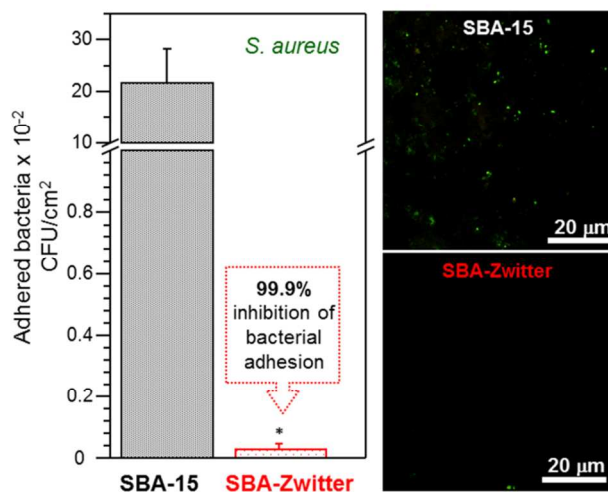
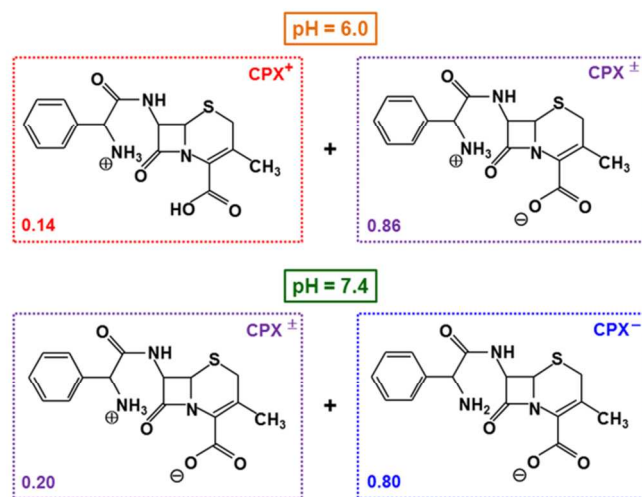


Fig. 8. Left: Counting of *S. aureus* forming colonies units after 90 minutes of culture onto SBA-15 and SBA-Zwitter surfaces. Statistical significance: \* $p < 0.01$ . Right: Confocal fluorescence micrographs of adhered *S. aureus* onto SBA-15 and SBA-Zwitter surfaces after staining with BacLight® Kit™.

There are regions exhibiting significantly less green fluorescence, which could be due to the presence of bacteria with slightly damaged membranes. Nonetheless, red fluorescence is not observed, which indicates that most of bacteria adhered remain viable onto the surface of SBA-15, *i.e.* this material does not produce bactericidal effect during the 90 min of adhesion assay. On the contrary, SBA-Zwitter surface exhibits minimal fluorescence, (Fig. 8). In fact there are only very small regions where green fluorescence can be detected. The presence of  $>\text{NH}_2^{\oplus}/-\text{SiO}^{\ominus}$  and  $-\text{NH}_3^{\oplus}/-\text{SiO}^{\ominus}$  *zwitterionic* pairs onto the surface of SBA-Zwitter would be hindering the adhesion of *S. aureus*. The small zones showing green fluorescence could be due to small regions where amino groups remains unprotonated, in agreement with results derived from  $^1\text{H} \rightarrow ^{13}\text{C}$  CP/MAS solid state NMR. The qualitative results derived from confocal microscopy support the quantitative results derived from CFUs counting, where SBA-Zwitter inhibited up to a 99.9% the amount of adhered bacteria compared to pure silica SBA-15.

### *In vitro* antibiotic adsorption and release

To test the performance of SBA-Zwitter as controlled delivery system, the *zwitterionic* antibiotic cephalixin (CPX) was selected and *in vitro* loading and release assays were performed. For comparison, *in vitro* CPX loading and delivery tests were performed in parallel using SBA-15 as host matrix. Loading assays were carried out by soaking powdered samples in water (pH ~ 6).<sup>52</sup> Elemental chemical analyses were used to quantify the amount of CPX loaded into the different mesoporous samples. The results are shown in Table 4, being 11.2 and 12.7 mg/g the amounts of CPX loaded for SBA-15 and SBA-Zwitter, respectively. It should be noticed that the relative small amount of CPX loaded, ~1% in both materials, is not expected to modify the chemical nature of the host matrices. In fact,  $\zeta$ -potential values at pH 7.4 of CPX-loaded samples were *ca.* 0 mV and -20 mV for SBA-Zwitter and SBA-15, respectively. These values are similar to those found for materials before CPX-loading. This fact is especially relevant in the case of SBA-Zwitter, where the *zwitterionic* nature of its surface needs to be preserved to inhibit bacterial adhesion.



**Fig. 9.** Cephalixin species at their relative abundance at the pH values of 6.0 (up) and 7.4 (down), where CPX<sup>+</sup>, CPX<sup>±</sup> and CPX<sup>-</sup> stand for the cationic, *zwitterionic* and anionic cephalixin species, respectively.

The main driving forces contributing to the adsorption of molecules on mesoporous silica can be regarded as electrostatic or Coulombic interaction, hydrogen bonding and non-polar interaction.<sup>30</sup> Herein, the non-polar interaction may be overruled due to the hydrophilic nature of both CPX and mesoporous matrices synthesized in this work. In aqueous media, CPX molecule exhibits different ionization states depending on the pH due to the presence of one carboxylic acid group and one amino group into its structure (Fig. 9).<sup>53</sup> At the loading pH of 6, 86% of CPX is found as *zwitterionic* specie (CPX<sup>±</sup>), where amino group is protonated as  $-\text{NH}_3^+$  and carboxylic acid group is deprotonated as  $-\text{COO}^-$ . Therefore, only 14% of CPX molecules would exist as positively charge

species (CPX<sup>+</sup>). On the other hand, Fig. 6 provides information about the estimated net surface charge of mesoporous samples. Thus, at pH = 6 SBA-15 and SBA-Zwitter exhibit  $\zeta$ -potential values of *ca.* -14 and +21 mV, respectively. *Zwitterionic* CPX<sup>±</sup> is capable of interacting through its protonated amino groups with deprotonated silanol groups in the surface of SBA-15 via electrostatic interactions ( $-\text{NH}_3^+ \cdots \text{OSi}^-$ ). On the other hand, since there are remaining Si-OH groups onto SBA-15 surface, hydrogen bond interactions with deprotonated carboxylic acid groups from CPX<sup>±</sup> ( $-\text{COO}^- \cdots \text{HO-Si-}$ ) could take place. Besides this type of interactions, which is also present between CPX and SBA-Zwitter sample, additional host-guest attracting forces occurs. Thus, CPX<sup>±</sup> is capable of interacting with the positively charged SBA-Zwitter surface via electrostatic attracting interactions between protonated amino groups from DAMO and deprotonated carboxylic acid groups from CPX ( $>\text{NH}_2^+ \cdots \text{OOC}^-$  and  $-\text{NH}_3^+ \cdots \text{OOC}^-$ ). These additional attractive electrostatic interactions would account for the slight higher CPX loading capability of SBA-Zwitter than that of SBA-15, despite of the higher surface area of the latter.

*In vitro* release tests were carried out in PBS at pH 7.4 and 37 °C. Fig. 10 shows CPX release patterns from both mesoporous matrices at the physiological pH of 7.4. Sustained drug release profiles are observed in all cases. For porous matrices it has been reported that drug release can be mediated by diffusion, erosion/degradation and swelling followed by diffusion.<sup>53</sup>

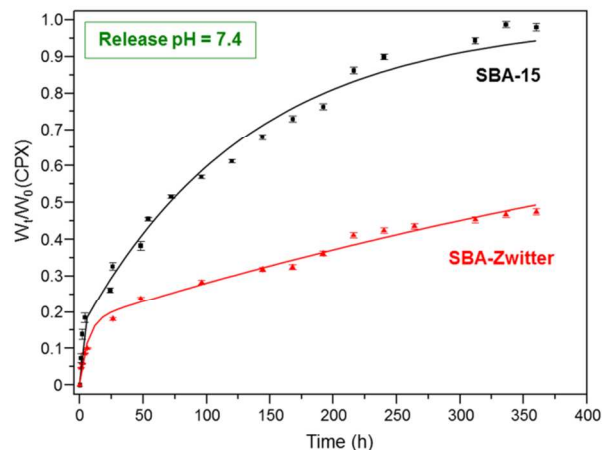


**Fig. 10.** Cephalixin (CPX) release profiles at pH 7.4 (phosphate buffer, PBS) for SBA-15 and SBA-Zwitter samples. Error bars represent the standard deviation for three measurements ( $N = 3$ ).

In fact, drug release is a combination of these three mechanisms with different modes of erosion: surface and bulk erosion. Although some matrix erosion and dissolution are involved, under perfect sink conditions, the main driving force for drug departure out of the mesoporous matrices is pore diffusion /

Table 4. Kinetic release parameters for cephalexin (CPX) release from SBA-15 and SBA-Zwitter materials.

Sample	W <sub>0</sub> (mg/g)	k <sub>off</sub> (×10 <sup>3</sup> )(h <sup>-1</sup> )	ΔG (10 <sup>-21</sup> J)	K <sub>s</sub> (h <sup>-1</sup> )	R <sup>2</sup>
SBA-15	11.2	7.4 ± 3.0	-7.5 ± 2.9	0.77 ± 0.34	0.994
SBA-Zwitter	12.7	1.51 ± 0.09	-7.0 ± 0.9	0.18 ± 0.3	0.993

convection, which can be fitted to first order kinetics. In addition to the diffusion-driven transport of drug molecules drug-carrier host-guest interactions are key factors to dictate drug release profiles.<sup>23,55</sup> Drug molecules may directly interact with mesoporous materials, lowering their solubility and/or retarding their release. In this case, drug molecules are termed as associated, which need to be disassociated from nanocarriers prior to release. The association and disassociation processes are assumed to be reversible. Furthermore, the reversible association of a drug molecule with a carrier is assumed to follow first order kinetics. Therefore, the theoretical model adopted in this work considers first-order diffusion/convection and drug association/disassociation.<sup>55</sup> Concretely, drug release patterns correspond to fast diffusion/convection but slow association/dissociation. This leads to a decoupling of drug association/disassociation from drug diffusion/convection: the fast release of initially free drug molecules via diffusion/convection and the slow release of initially bound drug molecules that is dictated by the disassociation process. Accordingly, two first order kinetics or two exponential release mechanisms can be described as follows:<sup>55</sup>

$$\frac{M_t}{M_0} = \frac{k_{off}}{k_{on}+k_{off}}(1 - e^{-k_s t}) + \frac{k_{on}}{k_{on}+k_{off}}(1 - e^{-k_{off} t}) \quad (\text{Eq. 5})$$

where  $M_t$  is the cumulative drug release at time  $t$ ;  $M_0$  is the initial amount of drug;  $k_s$  is the rate constant of diffusion/convection; and  $k_{on}$  and  $k_{off}$  are the rate constants of association and disassociation, respectively.

The free energy difference between the free and bound states,  $\Delta G$ , determines the amounts of initially free and bound drug, and can be calculated by the equation:

$$\Delta G = k_B T \ln \left( \frac{k_{on}}{k_{off}} \right) \quad (\text{Eq. 6})$$

where,  $k_B$  is the Boltzmann's constant and  $T$  is the absolute temperature (assumed to be 310 K). In this study, therefore, three parameters,  $\Delta G$  (instead of  $k_{on}$ ),  $k_s$  and  $k_{off}$  were used to describe the cumulative drug release from mesoporous silica materials.

Fitting experimental release patterns to Eq. 5 allowed us to determine the experimental values for  $k_s$ ,  $k_{on}$  and  $k_{off}$ . Then  $\Delta G$  was calculated using Eq. 6. The experimental results are summarized in Table 4. There is a good fitting of experimental results to the theoretical model ( $R^2 > 0.99$ ). The conditions  $k_s \gg k_{on}$  and  $k_s \gg k_{off}$  are fulfilled, which indicates that diffusion and convection are not neglected during the steady-state

release. Accordingly, drug release profiles can be classified as low initial burst release with steady-state release.<sup>56</sup>

Let's analyse the meaning of the different parameters derived from the fitting of experimental data to the theoretical model, which are displayed in Table 4.  $\Delta G$  gives us information about the magnitude of initial burst release. Fig. 10 shows a similar initial burst release of *ca.* 20% for both mesoporous materials. This is in very good agreement with the estimated value for  $\Delta G$ , being  $\sim 7 \times 10^{-21}$  J for both samples. The negative value of  $\Delta G$  accounts for increasing CPX-mesoporous matrix association, which reduces initial burst release and enhances steady state.  $k_s$  provides information about the rate of diffusion/convection, but not about the magnitude of the initial burst release. The model reveals a greater  $k_s$  value for SBA-Zwitter ( $\sim 0.18$  h<sup>-1</sup>) than that of SBA-15 ( $\sim 0.77$  h<sup>-1</sup>), which is the responsible of the prolonged initial burst release of the former. This indicates that CPX exhibits lower diffusivity in SBA-Zwitter than in SBA-15. Since the greater the pore diameter the faster the rate of drug diffusion from mesopores,<sup>23,57</sup> SBA-15 ( $D_p = 9.8$  nm) permits higher CPX diffusivity than SBA-Zwitter ( $D_p = 9.2$ ) (Table 2). The carrier-drug host-guest interactions can be related to the  $k_{off}$  value. Increasing  $k_{off}$  enhances steady release following initial burst release, but has no effect on the magnitude of initial burst release. The  $k_{off}$  value of SBA-Zwitter is almost 5-fold smaller ( $\sim 1.5 \times 10^{-3}$  h<sup>-1</sup>) than that of SBA-15 ( $\sim 7.4 \times 10^{-3}$  h<sup>-1</sup>) (Table 4). This is consistent with the existence of strong interactions between SBA-Zwitter and CPX, while weaker interactions occur between SBA-15 and CPX. At the physiological pH of 7.4, 80% of CPX exists in its anionic specie (CPX<sup>-</sup>), whereas only 20 % is present as *zwitterionic* molecule (CPX<sup>±</sup>). At such pH value, the surface charge of SBA-15 is negatively charged, whereas SBA-Zwitter is in *zwitterionic* form. Thus, repulsive electrostatic interactions between deprotonated silanol groups in SBA-15 and CPX<sup>-</sup> bearing  $-\text{COO}^-$  groups would predominate, which would trigger the CPX release from mesoporous matrix. On the contrary, electrostatic attractive interactions between primary and secondary protonated amino groups in SBA-Zwitter and  $-\text{COO}^-$  groups from CPX<sup>-</sup> would account for a more sustained drug release and lower  $k_{off}$  value for this functionalized material compared to pure silica SBA-15. Thus, after 15 days of assay almost 100% of CPX is released from SBA-15, while only 50% is released after the same time.

#### Agar disk-diffusion tests of cephalexin loaded materials

ADT allowed evaluating the capability of the CPX-loaded samples to eradicate *S. aureus* bacteria. CPX-free samples did not provoke inhibition zones during ADT, which accounts for their lack of bactericidal effect (Fig. S2, see supporting

information). On the contrary, well-defined inhibition zones were observed in the assays carried out with CPX-loaded samples. Thus, the inhibition zones were  $5.6 \pm 0.2$  and  $7.1 \pm 0.4$  mm for CPX-loaded SBA-15 and SBA-Zwitter samples, respectively. Such inhibition zones indicate that the amount of CPX diffused from both matrices during ADT exceeds the minimum inhibitory concentration (MIC) of *S. aureus* under these *in vitro* conditions. These results are in agreement with the *in vitro* delivery assays, where the amount of CPX released after 24 hours of assay is very similar in both samples (see Fig. 10). Note that the MIC value reported in the literature is 1–4  $\mu\text{g/mL}$  range depending on the *S. aureus* collection strain.<sup>58</sup> These results prove that the bactericidal capability of CPX is preserved after being submitted to the loading process into the different mesoporous samples.

## Conclusions

We have developed a bioceramic capable of decreasing relative bacterial adhesion from 100% to values lower than 0.1%, as derived from *in vitro* adhesion tests with *S. aureus*. This huge bacterial inhibition capability has not been previously reported for any mesoporous bioceramic at the physiological pH of 7.4. To attain this goal, the surface of SBA-15 has been provided of zwitterionic pairs ( $-\text{NH}_3^{\oplus}/-\text{SiO}^{\ominus}$  and  $>\text{NH}_2^{\oplus}/-\text{SiO}^{\ominus}$ ) by following the co-condensation route. A great antibiofouling capability is achieved due to the presence of very small amounts of functionalizing agent. This experimental result can be better understood thanks to current advanced techniques such as STEM-EDS, which permit the detection of almost negligible amounts of light elements such as nitrogen. *In vitro* loading and release assays using cephalexin as model antibiotic prove that zwitterionic SBA-15 can host drugs into its mesopores and release them over long time periods (more than 15 days). These are remarkable results that provide significant insights to design new bone implants capable of playing a dual role against infection. The zwitterionic nature permits inhibiting bacterial adhesion, which is the first stage of bone implant infection, whereas antibiotics release would help eradicating bacteria in the surroundings of the implant site.

## Acknowledgements

This study was supported by research grants from Ministerio de Ciencia e Innovación (MICINN) through the projects MAT2012-35556 and CSO2010-11384-E (Ageing Network of Excellence). Research by Marina Martínez-Carmona has been also supported by a PICATA predoctoral fellowship of the Moncloa Campus of International Excellence (UCM-UPM, ISCIII).

## Notes and references

<sup>a</sup> Departamento de Química Inorgánica y Bioinorgánica. Facultad de Farmacia, Universidad Complutense de Madrid. Instituto de Investigación

Sanitaria Hospital 12 de Octubre i+12. Plaza Ramón y Cajal s/n, 28040 Madrid, Spain.

<sup>b</sup> Center on Bioengineering, Biomaterials and Nanomedicine (CIBER-BBN), Spain

<sup>c</sup> CEI Campus Moncloa, UCM-UPM, Madrid, Spain.

<sup>d</sup> Departamento de Química Inorgánica, Facultad de Químicas, UCM, Spain.

\* Corresponding authors: mcolilla@ucm.es; vallet@ucm.es

† Electronic Supplementary Information (ESI) available: SEM micrographs and pore size distributions, determined by Hg intrusion porosimetry for disk-shaped SBA-15 and SBA-Zwitter samples. See DOI: 10.1039/b000000x/

1. D. Campoccia, L. Montanaro and C. R. Arciola, *Biomaterials*, 2013, **34**, 8018.
2. J. R. Edwards, K. D. Peterson, Y. Mu, S. Banerjee, K. Allen-Bridson, G. Morrell, M. A. Dudeck, D. A. Pollock and T. C. Horan, *Am. J. Infect. Control* 2009, **37**, 783.
3. J. D. M. D. Whitehouse, N. D. M. Friedman, K. B. M. D. Kirkland, W. J. M. D. Richardson and D. J. M. D. Sexton, *Infect. Control Hosp. Epidemiol.*, 2002, **23**, 183.
4. D. Arcos, A. R. Boccacini, M. Bohner, A. Díez-Pérez, M. Epple, E. Gómez-Barrena, A. Herrera, J. A. Planell, L. Rodríguez-Mañás and M. Vallet-Regí, *Acta Biomater.*, 2014, **10**, 1793.
5. C. E. Zobell, *J. Bacteriol.* 1943, **46**, 39.
6. J. Hasan, R. J. Crawford and E. P. Ivanova, *Trends Biotechnol.* 2013, **31**, 295.
7. X. Ding, C. Yang, T. P. Lim, L. Y. Hsu, A. C. Engler, J. L. Hedrick and Y.-Y. Yang, *Biomaterials*, 2012, **33**, 6593.
8. W. Heuer, A. Winkel, P. Kohorst, A. Lutzke, C. Pfaffenroth, H. Menzel, F. W. Bach, J. Volk, G. Leyhausen and M. Stiesch, *Adv. Eng. Mater.*, 2010, **12**, B609.
9. S. Jiang and Z. Cao, *Adv. Mater.*, 2010, **22**, 920.
10. I. Eshet, V. Freger, R. Kasher, M. Herzberg, J. Lei and M. Ulbricht, *Biomacromolecules*, 2011, **12**, 2681.
11. M. Colilla, I. Izquierdo-Barba, S. Sánchez-Salcedo, J. L. G. Fierro, J. L. Hueso and M. Vallet-Regí, *Chem. Mater.*, 2010, **22**, 6459.
12. I. Izquierdo-Barba, S. Sánchez-Salcedo, M. Colilla, M. J. Feito, C. Ramírez-Santillán, M. T. Portolés and M. Vallet-Regí, *Acta Biomater.*, 2011, **7**, 2977.
13. S. Sánchez-Salcedo, M. Colilla, I. Izquierdo-Barba and M. Vallet-Regí, *J. Mater. Chem. B*, 2013, **1**, 1595.
14. M. L. W. Knetsch and L. H. Koole, *Polymers*, 2011, **3**, 340.
15. D. M. Eby, K. E. Farrington and G. R. Johnson, *Biomacromolecules*, 2008, **9**, 2487.
16. I. Izquierdo-Barba, M. Vallet-Regí, N. Kupferschmidt, O. Terasaki, A. Schmidtchen and M. Malmsten, *Biomaterials*, 2009, **30**, 5729.
17. S. B. Lee, R. R. Koepsel, S. W. Morley, K. Matyjaszewski, Y. Sun and A. J. Russell, *Biomacromolecules*, 2004, **5**, 877.
18. M. Cicuéndez, I. Izquierdo-Barba, M. T. Portolés and M. Vallet-Regí, *Eur. J. Pharm. Biopharm.*, 2013, **84**, 115.
19. D. Molina-Manso, M. Manzano, J. C. Doadrio, G. del Prado, A. Ortiz-Pérez, M. Vallet-Regí, E.; Gómez-Barrena and J. Esteban, *Int. J. Antimicrob. Agents*, 2012, **40**, 252.
20. M. Vallet-Regí, M. M. García and M. Colilla, *Biomedical Applications of Mesoporous Ceramics. Drug Delivery, Smart Materials*

- and Bone Tissue Engineering. CRC Press, Taylor & Francis: New York, USA, 2013.
21. D. Arcos, M. and Vallet-Regí, *Acta Mater.*, 2013, **61**, 890.
22. M. Manzano, M. Colilla and M. Vallet-Regí, *Expert Opin. Drug Deliv.*, 2009, **6**, 1383.
23. M. Vallet-Regí, F. Balas and D. Arcos, *Angew. Chem. Int. Ed.*, 2007, **46**, 7548.
24. M. Vallet-Regí and E. Ruiz-Hernández, *Adv. Mater.*, 2011, **23**, 5177.
25. D. L. Slomberg, Y. Lu, A. D. Broadnax, R. A. Hunter, A. W. Carpenter and M. H. Schoenfish. *Appl. Mater. Interfaces*, 2013, **5**, 9322-9329.
26. Y. Lu, D. L. Slomberg, B. Sun and M. H. Schoenfish, *Small*, 2013, **9**, 2189-2198.
27. G. Cheng, H. Xue, Z. Zhang, S. Chen and S. Jiang, *Angew. Chem. Int. Ed.*, 2008, **47**, 8831.
28. Z. Cao, L. Mi, J. Mendiola, J. -R. Ella-Menye, L. Zhang, H. Xue and S. Jiang, *Angew. Chem. Int. Ed.*, 2012, **51**, 2602.
29. F. Hoffmann, M. Cornelius, J. Morell and M. Fröba, *Angew. Chem. Int. Ed.*, 2006, **45**, 3216.
30. A. Nieto, M. Colilla, F. Balas and M. Vallet-Regí, *Langmuir* 2010, **26**, 5038.
31. D. Zhao, J. Feng, Q. Huo, N. Melosh, G. H. Fredrickson, B. F. Chmelka and G. D. Stucky, *Science*, 1998, **279**, 548.
32. W. Whitnall, T. Asefa and G. A. Ozin, *Adv. Funct. Mater.* 2005, **15**, 1696.
33. S. Brunauer, P. H. Emmett and E. Teller, *J. Am. Chem. Soc.*, 1938, **60**, 309.
34. S. J. Gregg and K. S. W. Sing, *Adsorption, surface area, and porosity*. Academic Press: London, New York, 1982.
35. E. P. Barrett, L. G. Joyner, P. P. Halenda, *J. Am. Chem. Soc.*, 1951, **73**, 373.
36. M. Kruk, M. Jaroniec and A. Sayari, *Chem. Mater.*, 1999, **11**, 492.
37. B. H. Wouters, T. Chen, M. Dewilde and P. J. Grobet, *Microporous Mesoporous Mater.*, 2001, **44-45**, 453.
38. G. Cheng, Z. Zhang, S. Chen, J. D. Bryers, S. Jiang, *Biomaterials*, 2007, **28**, 4192.
39. M. Katsikogianni and Y. F. Missirlis, *Eur. Cells Mater.*, 2004, **8**, 37.
40. T. J. Kinnari, J. Esteban, N. Z. Martín-de-Hijas, O.; Sánchez-Muñoz, S. Sánchez-Salcedo, M.; Colilla, M. Vallet-Regí and E. Gómez-Barrena, *J. Med. Microbiol.* 2009, **58**, 132.
41. T. J. Kinnari, J. Esteban, E. Gómez-Barrena, N. Zamora, R. Fernández-Roblas, A. Nieto, J. C. Doadrio, A. López-Noriega, E. Ruiz-Hernández, D. Arcos and M. Vallet-Regí, *J. Biomed. Mater. Res. A*, 2009, **89A**, 215.
42. V. E. Wagner, J. T. Koberstein and J. D. Bryers, *Biomaterials*, 2004, **25**, 2247.
43. E. W. Washburn, *Proc. Natl. Acad. Sci. USA*, 1921, **7**, 115.
44. L. Boulos, M. Prévost, B. Barbeau, J. Coallier and R. Desjardins, *J. Microbiol. Meth.*, 1999, **37**, 77.
45. S. Imazatoa, A. Kuramotoa, Y. Takahashia, S. Ebisua, M. C. Peters. *Dental Mater.*, 2006, **22**, 527.
46. M. Vallet-Regí, M. Colilla and B. González, *Chem. Soc. Rev.*, 2011, **40**, 596.
47. C. J. Brinker, *Sol-gel science: the physics and chemistry of sol-gel processing*, Academic Press: Boston, 1990.
48. M. Colilla, A. J. Salinas and M. Vallet-Regí, *Chem. Mater.* 2006, **18**, 5676.
49. M. Colilla, M. Darder, P. Aranda and E. Ruiz-Hitzky, *J. Mater. Chem.*, 2005, **15**, 3844.
50. J. J. Yang, I. M. El-Nahhal, I. S. Chuang and G. E. Maciel, *J. Non-Cryst. Solids*, 1997, **209**, 19.
51. S. Chen, L. Li, C. Zhao and J. Zheng, *Polymer*, 2010, **51**, 5283.
52. M. S. Legnoverde, I. Jiménez-Morales, A. Jiménez-Morales, E.; Rodríguez-Castellón and E. I. Basaldella, *Med. Chem.*, 2013, **9**, 672.
53. M. S. Legnoverde, S. Simonetti and E. I. Basaldella, *Appl. Surf. Sci.* 2014, **300**, 37.
54. T. Ukmar, U. Maver, O. Planinšek, V. Kaučič, M. Gaberšček and A. Godec, *J. Control. Release*, 2011, **155**, 409.
55. L. Zeng, L. An and X. Wu, *J. Drug Deliv.* 2011, **2011**, 15.
56. M. Ye, S. Kim and K. Park, *J. Control. Release* 2010, **146**, 241.
57. M. Vallet-Regí, A. Rámila, R. P. del Real and J. Pérez-Pariente, *Chem. Mater.*, 2001, **13**, 308.
58. J.M. Andrews, *J. Antimicrob. Chemother.* 2001, **48**, 5.